JOURNAL OF AIRCRAFT
Vol. 41, No. 4, July–August 2004

Nonlinear Model Development from Flight-Test Data for F/A-18E Super Hornet

Alfonso C. Paris*
Science Applications International Corporation, Lexington Park, Maryland 20653
and
Michael Bonner†
Naval Air Systems Command, Patuxent River, Maryland 20670

Applied procedures for nonlinear aerodynamic model development and extraction from flight data for the F/A-18E Super Hornet aircraft are addressed. Parameter identification maneuver design, flight-test support technique, and aerodynamic model development are included. All-axis 3–2–1–1 maneuvers were designed to best excite the longitudinal and lateral–directional system natural frequencies of interest. The work was in support of leading edge flap degraded modes studies for the F/A-18E aircraft investigated by the Naval Air Systems Command. In this flight-test program, the effect of off-schedule, differentially frozen, leading-edge flaps was examined with the aircraft in power-approach configuration. A variety of processes was employed to develop fully nonlinear longitudinal and lateral–directional aerodynamic incremental model corrections. This effort included total aerodynamic coefficient reconstruction from flight-test data and equation error analysis for model structure development/estimation. The available data allowed for the successful extraction of incremental coefficients for aerodynamic forces and moments that resulted in an engineering simulation with increased aerodynamic fidelity in the configurations examined.

Introduction

THE F/A-18E is a twin-engine U.S. Navy aircraft produced by The Boeing Company. During a normal approach to landing, the F/A-18 schedules leading-edge flap (LEF) deflection with angle of attack (AOA) to optimize lift. The trailing-edge flaps are symmetrically deflected 30 deg down. This configuration is referred to as powered-approach half-flaps (PA-half). Failures of the LEF drive unit while in this configuration were of concern due to the potential for lift loss and asymmetric lift if only one side fails while at low altitude. A flight-test program was designed to collect pilot handling qualities assessments of this degraded configuration, as well as parameter identification (PID) data for use in updating the engineering aerodynamic model.

Flights performed in the fall of 2001 at Naval Air Station Patuxent River resulted in the collection of flight-test data appropriate for PID purposes. Specifically, flight-test data analyzed in this study were collected in PA-half configuration with gear extended. The aircraft loading examined in this paper is the fighter centerline tank (FCL) configuration. A similar analysis took place for the interdiction three tank (INT3) configuration. Available PID flight data spanned an AOA range of 4–10 deg.

Data archival, preprocessing, and PID analysis were performed within the integrated data evaluation and analysis system (IDEAS) developed by Science Applications International Corporation. IDEAS is a powerful database management system and analysis software containing a full complement of flight data preprocessing, calibration, simulation, model estimation, model verification, and validation tools.[1,2]

Received 17 June 2003; presented as Paper 2003-5535 at the AIAA 2003 AFM Conference, Austin, TX, 11–14 August 2003; revision received 9 December 2003; accepted for publication 10 December 2003.

*Aerospace Engineer, Simulation and Research Services Division, 22299 Exploration Drive, Suite 200; alfonso.paris@saic.com. Member AIAA.
†Aerospace Engineer, NAVAIR, Flight Vehicle Simulation Branch (AIR-4.3.2.3), Building 2035, Room 118, Naval Air Station Patuxent River; michael.bonner@navy.mil. Member AIAA.

Flight-test data collected for the purpose of aerodynamic parameter estimation typically consist of inertial and air-relative sensor outputs. Before performing PID analyses, or traditional data reduction, it was important to evaluate, and if necessary correct, the measured data to ensure kinematic consistency amongst them. Consequently, a rigorous postflight data calibration study was performed within IDEAS using the navigation identification (NAVIDNT) tool. This tool couples an adaptive nonlinear least-squares identification algorithm (LSIDNT) with a set of rigid-body navigation equations that model aircraft motion over an oblate, rotating Earth.[1,3,4] Sensor biases and/or scale factors, as well as time-invariant atmospheric winds, may be identified using this tool.

Additional data preprocessing resulted in engine thrust information for each PID maneuver. Given this information, tools within IDEAS allowed for the extraction of total aerodynamic force and moment coefficient histories for each maneuver.

Test data from maneuvers of comparable configuration were placed into analysis groups with ample data made available to span a suitable range of the flight-test envelope investigated. Aerodynamic model structures were developed through analysis of these groups using an equation error extraction technique in IDEAS known as Athena employing principal component axis regression. Athena expresses the overall aerodynamic forces and moments as linear combinations of parameters such as stability derivatives and/or increments. In addition, to develop parameter nonlinearities, Athena supports the use of linear or cubic basis splines. The resulting model was installed in an engineering simulation for the F/A-18E airframe at the manned flight simulator (MFS) facility of the U.S. Naval Air Systems Command (NAVAIR) at Naval Air Station Patuxent River. This simulation is hosted within the controls analysis and simulation test loop environment (CASTLE) developed by the U.S. Navy.[5] Regions outside the identified incremental model envelope were emulated by holding table output constant to their appropriate endpoint values.

Overall, PID analysis resulted in incremental updates for aerodynamic body axis X, Y, and Z forces as well as pitching, rolling, and yawing moment coefficients.

Each of the total aerodynamic coefficients follow a similar basic structure in that they consist of a sum of incremental effects. These contributions include effects due to a basic, or bias, aerodynamic coefficient, air-relative orientation, aircraft body axis angular rates, and control surface positions.

The following sections examine the maneuver design, data preprocessing, model structure development, and aerodynamic model extraction techniques in detail.

Maneuver Design

The primary dynamic maneuver chosen to excite aerodynamic modes of interest for this program was the 3–2–1–1 multistep input. This input has been used in a number of PID programs due to its relative ease of performance by the pilot and the enhanced information content relative to classical doublets.[6–10]

The 3–2–1–1 consists of equal amplitude, opposite sign step inputs of duration $3 \times T_C$, $2 \times T_C$, $1 \times T_C$, and $1 \times T_C$. The 3–2–1–1 characteristic time T_C is selected such that the peak frequency content of the input matches the aircraft natural response frequency for the flight condition being tested. Empirically, the peak frequency of the 3–2–1–1 is centered near the frequency corresponding to the 2 portion of the input. Based on this, the relationship between peak spectral frequency in hertz and characteristic time can be easily derived,

$$T_C = 0.25/f_{\text{target}} \tag{1}$$

This relationship was verified using the MATLAB® analysis software package, by computing power spectral densities for a range of T_C and fitting a curve to the resulting peak frequency vs T_C plot. This experimental approach resulted in a relationship very similar to the preceding one,

$$T_C = 0.35/f_{\text{target}} \tag{2}$$

The variation in timing and the step reversals in the 3–2–1–1 results in broad frequency content in the input, rather than the sharp peak typical of classical doublets. This allows some leeway in input design and execution because it is not necessary to match exactly the target input frequency or timing to get sufficient output excitation.

Aircraft natural frequencies at the flight conditions of interest were determined from Boeing Aircraft Corporation documentation.[11] Aircraft closed-loop natural frequencies for the tested configuration ranged from 1.25 to 2.0 rad/s for the longitudinal modes and from 1.75 to 2.5 rad/s for the lateral–directional modes. The resulting 3–2–1–1 characteristic times ranged from 1.8 to 1.1 s for the longitudinal modes and 1.3 to 0.9 s for the lateral–directional modes. When it was recognized that small differences in timing would be indistinguishable to the pilot, three characteristic times were selected to cover the required frequency range: 0.9, 1.4, and 1.8 s. Each input was evaluated before actual flight using an existing high-fidelity desktop simulation. Because the 1.8-s input was only specified for a single longitudinal input condition and resulted in excessive deviation from the nominal condition during simulation testing, it was dropped from the test matrix, leaving the 0.9- and 1.4-s inputs.

Based on simulation studies using the Boeing/NAVAIR F/A-18 engineering simulation, input amplitudes of 25–33% of full input throw were specified in each axis. Inputs of these magnitudes provided sufficient excitation for system identification analysis, while limiting excursions from the nominal conditions. In addition, to further control excursions from nominal test conditions, the amplitude of the initial input for each 3–2–1–1 was reduced 50% relative to the remaining inputs.

Experience in previous programs has shown that pilots are better able to execute the 3–2–1–1 when they have practiced it in a simulator before flight test.[9] The MFS facility at U.S. Naval Air Warfare Center Aircraft Division Patuxent River, Maryland was utilized for pilot and test team practice. An audio microsoft waveform file played over the intercom system provided pilot cuing. The audio cuing consisted of a series of beeps at alternating frequency, with each beep designating an input reversal point. In addition to maneuver practice, the pilots also evaluated various cuing techniques, such as memorizing the tones or "chasing" the tones. Initially, the selected tone sequence was played for the pilot to get a feel for the timing. The pilot would then perform the 3–2–1–1 from memory. Alternately, the pilot would chase the tones, that is, perform the input in direct response to the beeps. Based on preflight simulation experience the test pilots in this program preferred to chase the tones. During the actual test flights, the audio cues were uplinked to the pilot over the aircraft radio. This resulted in very good maneuver repeatability and low variation from the design input timing.

It is important to stress the need for single-axis inputs, even when using experienced test pilots. During the postflight briefing after the initial test flight, the pilot stated that the longitudinal 3–2–1–1 was a difficult maneuver to execute, because it was necessary to modulate the throttle to maintain AOA while deflecting the stick. U.S. Navy pilots are taught to maintain AOA on approach to landing by modulating the throttle. Consequently, the pilot was following, albeit erroneously, standard operating procedures. Unfortunately, this is not at all desirable for a longitudinal PID maneuver because AOA excitation is the goal. During all following preflight briefings, the test team specifically requested "no throttle movement" during the longitudinal inputs.

One other difficulty that arose during the maneuver design process was related to the required accuracy of the 3–2–1–1 inputs. The flight-test team did not have experience with the 3–2–1–1 input and requested tolerances to define maneuver acceptability. However, a desirable feature of the 3–2–1–1 is the relatively loose requirement on input amplitude and phasing. In fact, it is desirable to have some variation from the exact 3–2–1–1 timing to increase frequency content in the input signal. However, the test team was accustomed to specifying hard and fast tolerances on time and input magnitudes to define "acceptable" inputs. After much discussion, an acceptable set of broad input timing tolerances was developed. Input amplitude tolerances were based on test planning safety criteria and in-flight monitoring of adequate airframe response.

A critical component of this program was the presence of PID engineers in the control and monitoring room during the actual test flights. This allowed the data "customer" to assist in real-time evaluation of the maneuvers as they were performed. Test team concerns over maneuver acceptability were alleviated because the PID engineers were present and could evaluate maneuver quality real time. This practically eliminated the need to repeat maneuver blocks on subsequent flights due to insufficient excitation or deviation from nominal condition.

Available Flight-Test Maneuvers

A variety of maneuvers were flown during these studies to allow for collection of flying quality information in the degraded mode configurations of interest. Maneuvers examined for aerodynamic model extraction purposes include pilot-applied all-axis 3–2–1–1s and steady heading sideslips (SHSS). Maneuvers were performed in blocks at each aircraft configuration and AOA investigated. Again, the aircraft configuration study outlined in this paper is FCL in PA-half with landing gear extended. LEF splits of (L/R) $-5/5$ deg, $0/5$ deg, $10/5$ deg, $20/5$ deg, and $34/5$ deg were investigated. These flap splits were chosen based on design characteristics of the flight control system. A LEF failure typically results in the good LEF being driven to 5 deg, whereas the failed LEF will remain at some arbitrary deflection. An overall AOA range of 4–10 deg was tested for each LEF split case.

Each maneuver block utilized in this PID study contained the following maneuvers, flown back to back, for each flight condition and aircraft configuration: longitudinal stick 3–2–1–1, lateral stick 3–2–1–1, directional pedal 3–2–1–1, and SHSS and release.

Flight conditions examined were at 4-, 6-, 8-, and 10-deg AOA. The all-axis 3–2–1–1s were designed to excite the aircraft short-period and Dutch roll natural frequencies, making available information content appropriate for PID purposes. The SHSS maneuvers provide additional information regarding directional stability, lateral–directional control power, and longitudinal affects in sideslip. The SHSS maneuvers were particularly important in defining effects on these parameters due to the asymmetric configurations investigated. The SHSS tests were flown in both the positive and negative sideslip condition due to the asymmetric LEF configurations. Pilot pedal input was applied gradually to full while lateral stick cross control was applied to maintain aircraft heading. The pilot

held the full pedal condition for a short time, maintaining a static trim condition, followed by an abrupt release of lateral stick and pedal to neutral to exercise the aircraft dynamic recovery response. Although additional flying quality style maneuvers were available, such as pitch attitude and roll attitude captures, PID analysis was limited to those mentioned earlier.

AOA excursions during the longitudinal 3–2–1–1 inputs were typically ±3–4 deg, whereas N_z variations were typically ±0.3 g at the 4-deg AOA case, decreasing to ±0.1 g at 10-deg AOA. For the lateral 3–2–1–1 inputs, peak-to-peak bank angle changes totaling 60–80 deg were typically generated. At the 10-deg AOA test condition, the total bank angle excursions were 30–50 deg. The bank angle changes were generally not symmetric about wings level due to the asymmetric nature of the split LEF test configuration. The directional 3–2–1–1 inputs typically generated 3–5 deg of total sideslip excursion and ±−0.1 g of lateral acceleration. Again because of the asymmetric nature of the aircraft configuration, the sideslip excursions were generally not symmetric about zero. Sideslip excursions during the SHSS inputs ranged from ±5 to ±8 deg.

In the FCL study, a total of 84 individual PID maneuvers were separated into a series of longitudinal and lateral–directional analysis groups within IDEAS. Each group contained a collection of appropriate maneuvers from the preceding list that were flown under identical aircraft configuration and spanned a suitable AOA range for nonlinear model development purposes.

Such analysis groups are instrumental during the PID process in that they present a wealth of information, through a collection of PID maneuvers, to the estimation algorithm, allowing for the extraction of a global aerodynamic model.

Dynamic Flight-Test Data Preprocessing

The preprocessing procedure leading up to PID analysis is outlined in Fig. 1. Analysis within IDEAS examined pertinent channels from each maneuver for data dropouts and/or signal wrapping. Appropriate utilities within the IDEAS data preprocessing and reconstruction (DATPAR) toolbox were employed to correct such anomalies when they occurred.[1,2] Specifically, the DATPAR UNWRAP utility was used to generate continuous signals from discontinuous, wrapped, sensor outputs such as heading when necessary. In addition, the DATPAR WILD_EDIT utility was used to discard "wild points" from the flight-test data when encountered due to telemetry dropouts.

Prior analysis performed by Boeing engineers, regarding evaluation of the instrumentation system, resulted in a known set of required instrumentation time leads that were duly applied. Necessary time leads were applied to all flight control deflections, inertial navigation system (INS) angular rates, and linear accelerations.

Kinematic consistency evaluations were performed on all flight-test data using NAVIDNT within IDEAS. Recall that NAVIDNT couples the nonlinear least-squares algorithm LSIDNT with a set of navigation equations of motion to form an output error sensor model identification scheme.[1,3,4] The navigation equations integrate flight-measured linear accelerations and angular rates to generate rigid-body airframe responses. The goal of this process, of course, is to ensure all accelerations, rates, angular orientations, and inertial positions are consistent. Recall that NAVIDNT is used to estimate sensor biases and/or scale factors, as well as time-invariant atmospheric winds, to generate a kinematically consistent dataset. LSIDNT, the optimizer, is a robust, adaptive nonlinear least-squares scheme based on the N2F family of algorithms encompassing the Newton minimization scheme with an augmented version of the Gauss–Newton approximation (see Ref. 4). NAVIDNT studies within IDEAS indicated the data to be kinematically consistent with no biases and/or scale factors required for application against the sensors in question. However, during the calibration procedure within IDEAS, the kinematically consistent traces reconstructed by NAVIDNT for AOA and angle of sideslip were to be used later during PID analysis. The INS computed AOA/angle of sideslip available in the flight data were shown to lag the corresponding traces generated by NAVIDNT in the kinematically consistent data set by approximately 100 ms. This is not surprising in that INS signals for AOA and angle of sideslip are computed entities rather than direct measurements, which adds an inherent delay in itself, in addition to any delay in their being officially recorded. Consequently, the AOA and angle of sideslip reconstructed by NAVIDNT were to be used in the PID analysis.

Finally, DATPAR tools were used to compute a variety of important histories for each maneuver including air relative velocities, air relative body-axis accelerations, flow angle rates, equivalent control surface deflections, and sign convention/units bookkeeping.[1,2]

Total Aerodynamic Force and Moment Reconstruction

A variety of data is necessary to extract total aerodynamic force and moment coefficients successfully from flight data. These data consist of body-axis angular rates and accelerations, body-axis linear accelerations, dynamic pressure, body-axis thrust-produced forces and moments, as well as aircraft mass and inertia data. In addition, to facilitate transferring the overall moments to a specific reference point, about which the aerodynamic model is to be developed, the center of gravity location for each maneuver must be determined.

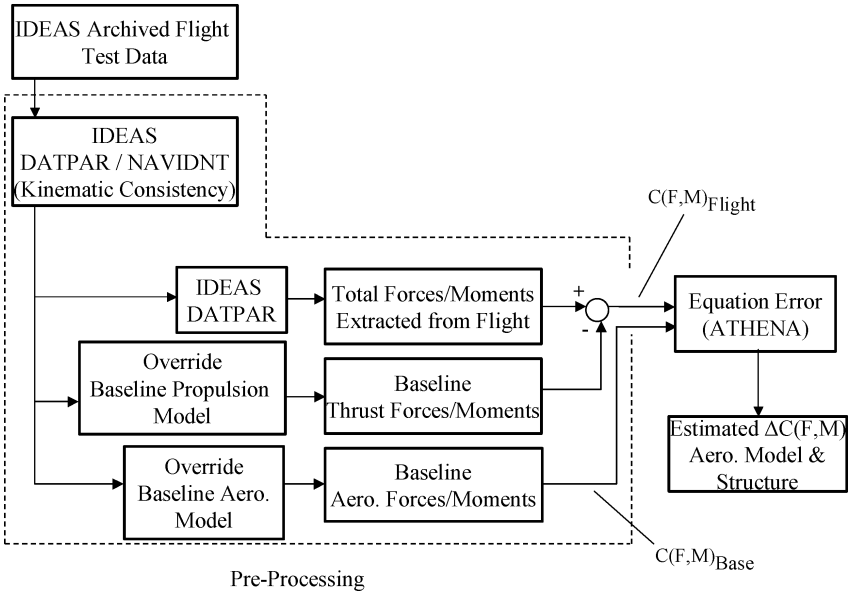

Fig. 1 Flight-test data preprocessing and incremental aerodynamic model development procedure.

Appropriate angular rate, angular acceleration, linear acceleration, and dynamic pressure data were available in the flight-test data and subject to DATPAR preprocessing as outlined earlier. Suitable information regarding aircraft weight and balance characteristics such as mass, center-of-gravity position, and moments of inertia were readily available within the provided flight-test data. Body-axis thrust forces and moments were reconstructed because they were not available in the provided data.

Thrust body-axis forces and moments about the aircraft c.g. for each maneuver were determined using the available F/A-18E/F propulsion model in the overall CASTLE engineering simulation. To accomplish this, the propulsion model was run independently with all pertinent inputs to the engine model being substituted with flight-test data. This is known as overriding input terms within a simulation module. Flight data for throttle positions, engine fan speeds, engine core speeds, and other required aircraft states and responses stored in IDEAS were used to override pertinent input variables within the propulsion simulation. Resulting thrust body-axis forces and moments were recorded from the simulation and stored within IDEAS. Note that the current software engine model has not yet been validated against flight-test data. Any region of degraded fidelity in the software engine model will impact the total aerodynamic coefficients, primarily drag, that can be extracted. However, this currently accepted F414-400 software engine model is built on static thrust lookup tables from engine manufacturer data. Installation and gyroscopic effects are modeled in the simulation. Engine dynamics are modeled by applying lag filters to the table lookup outputs. All PID maneuvers were flown with throttles maintained at their trim position throughout each maneuver.

A variety of IDEAS DATPAR tools were employed to extract the total aerodynamic force and moment coefficients from the flight data.[1,2] This resulted in the overall aerodynamic body axis X, Y, and Z forces, as well as pitching moment, rolling moment, and yawing moment coefficient histories with respect to the aircraft c.g. per PID maneuver. Overall, IDEAS DATPAR utilities were used to back calculate the aircraft body axis aerodynamic forces and moments given pertinent measured airframe linear and angular accelerations, airframe states, weight and balance information, as well as predicted propulsion forces and moments. All aerodynamic body-axis total coefficients were reconstructed assuming a rigid-body aircraft.

An additional IDEAS DATPAR utility was used to transfer all reconstructed body-axis aerodynamic moments to the desired reference point about which the aerodynamic model would be developed.[1,2] This transference involves the incremental effects due to the reconstructed body-axis aerodynamic forces about the aircraft c.g. being offset from the desired aerodynamic reference center location.

The total aerodynamic forces and moments predicted by the current baseline aerodynamic model are of importance as well. When compared to those reconstructed from flight-test data, they offer clues as to where model improvement is required. In addition, they act as a baseline themselves when developing the incremental aerodynamic model. The predicted baseline aerodynamic forces and moments are obtained in a similar fashion to the override technique earlier outlined to determine predicted thrust forces and moments. The baseline aerodynamic model was run independently in the airframe simulation with all pertinent module inputs being replaced with aircraft states, responses, and control surface positions recorded during flight. Resulting predictions for the baseline total aerodynamic forces and moments were then recorded and stored within IDEAS.

Again, a general overview of these analysis procedures may be seen in Fig. 1.

Aerodynamic Model Structure Development and Identification Using Equation Error

Estimation Algorithm

The next stage of analysis involved an equation error PID technique to extract an incremental aerodynamic model for the F/A-18E in the split LEF degraded modes configurations. The equation error tool in IDEAS, known as Athena, is capable of determining the overall aerodynamic force and moment models as linear combinations of parameters (typically stability derivatives and/or incremental coefficients) using a principal component regression algorithm.[1,2,12,13] In addition, Athena allows these terms to be modeled with nonlinear dependencies. As an example, consider a very simple pitching moment buildup,

$$C_m = C_{m\,\text{basic}}(\alpha) + C_{m\delta e}(\alpha) \cdot \delta_e \tag{3}$$

In this example, the overall model structure is a nonlinear function of AOA. To model the nonlinearities, Athena supports the use of linear or cubic basis splines to estimate linear coefficients of the splines at the specified knot locations of the nonlinear function. Equation (3) is rewritten as

$$C_m = \sum_{i=1}^{K1} C_{m\,\text{basic},i} \cdot f_{1,i}(\alpha) + \sum_{i=1}^{K2} C_{m\delta e,i} \cdot f_{2,i}(\alpha) \cdot \delta_e \tag{4}$$

$C_{m\,\text{basic},i}$ and $C_{m\delta e,i}$ are the parameters to be estimated; $K1$ and $K2$ are the number of AOA knot locations defined for $C_{m\,\text{basic}}$ and $C_{m\delta e}$, respectively; and $f_{1,i}(\alpha)$ and $f_{2,i}(\alpha)$ are basis functions. Typically, the basis functions are defined such that each takes on a value of 1.0 at one knot location and a value of 0.0 at all other knot locations.

Athena assumes the model may be represented as a set of linearly combined, time-independent linear parameters with the following structure:

$$\boldsymbol{y} = \boldsymbol{A}\boldsymbol{p} + \boldsymbol{v} \tag{5}$$

Vector $\boldsymbol{y}$ (size $n \times 1$) represents the total nondimensional force or moment coefficient history vector under investigation. The parameter vector $\boldsymbol{p}$ (size $m \times 1$) represents the stability and control derivatives under estimation, and the regressor matrix $\boldsymbol{A}$ (size $n \times m$) contains the independent variables. Vector $\boldsymbol{v}$ (size $n \times 1$) represents unmodeled aerodynamic responses and/or phenomena such as due to system/sensor noise. Consider the example outlined by Eqs. (3) and (4) assuming two AOA knot locations are chosen for both $C_{m\,\text{basic}}$ and $C_{m\delta e}$. In this case, Eq. (5) becomes

$$\begin{bmatrix} C_m(1) \\ \vdots \\ C_m(n) \end{bmatrix} = \begin{bmatrix} f_{1,1}(\alpha(1)) & f_{1,2}(\alpha(1)) & f_{2,1}(\alpha(1)) \cdot \delta_e(1) & f_{2,2}(\alpha(1)) \cdot \delta_e(1) \\ \vdots & \vdots & \vdots & \vdots \\ f_{1,1}(\alpha(n)) & f_{1,2}(\alpha(n)) & f_{2,1}(\alpha(n)) \cdot \delta_e(n) & f_{2,2}(\alpha(n)) \cdot \delta_e(n) \end{bmatrix} \times \begin{bmatrix} C_{m\,\text{basic},1} \\ C_{m\,\text{basic},2} \\ C_{m\delta e,1} \\ C_{m\delta e,2} \end{bmatrix} + \begin{bmatrix} v(1) \\ \vdots \\ v(n) \end{bmatrix} \tag{6}$$

Athena uses a numerically robust singular value decomposition method to solve Eq. 5 and estimate the parameter vector $\boldsymbol{p}$. In general, Athena first determines an incremental response vector $\boldsymbol{y}_s$ by removing the prior model contributions, $\boldsymbol{p}_0$,

$$\boldsymbol{y}_s = \boldsymbol{y} - \boldsymbol{A}\boldsymbol{p}_0 \tag{7}$$

Vector $\boldsymbol{p}_0$ consists of a priori estimates, of parameters, as well as parameters that have been fixed and are not to be estimated. The regressor matrix $\boldsymbol{A}$ is then thinned such that it contains only those columns that correspond to parameters that are to be estimated. The thinned matrix $\boldsymbol{A}_s$ allows the identification statement of Eq. (5) to be reformulated as follows:

$$\boldsymbol{y}_s = \boldsymbol{A}_s\boldsymbol{p}_s + \boldsymbol{v} \tag{8}$$

The thinned regressor matrix $\boldsymbol{A}_s$ is then decomposed into the following form:

$$\boldsymbol{A}_s = \boldsymbol{USV}^T \tag{9}$$

where $\boldsymbol{U}$ and $\boldsymbol{V}$ are orthogonal and $\boldsymbol{S}$ is a diagonal matrix containing the singular values. When Eqs. (8) and (9) are used together, the free parameters are then estimated in principal component axes:

$$\boldsymbol{p}_s = \boldsymbol{VS}^{+}\boldsymbol{U}^T\boldsymbol{y}_s \tag{10}$$

Note that vectors $\boldsymbol{p}_0$ and $\boldsymbol{p}_s$ are combined to yield the final parameter estimates,

$$\boldsymbol{p} = \boldsymbol{p}_0 + \boldsymbol{p}_s \tag{11}$$

Output statistics for this technique are provided in the form of a fit percentage based on the Theil inequality coefficient statistic U defined as (see Ref. 14)

$$U = \frac{\sqrt{(1/N)\sum_{i=1}^{N}(\hat{y}_i - y_i)^2}}{\sqrt{(1/N)\sum_{i=1}^{N}(\hat{y}_i)^2} + \sqrt{(1/N)\sum_{i=1}^{N}(y_i)^2}} \tag{12}$$

N is the total number of points in the residual vector. This coefficient represents the ratio of the root-mean-square fit error and the root-mean-square values of the estimated and actual signal summed together. The value of U always falls between 0 and 1, where 0 indicates a perfect fit and 1 the worst fit.

The Athena fit percentage F, a measure of signal fit quality, is defined as follows:

$$F = 100(1 - U) \tag{13}$$

A 100% fit represents a perfect match with the measured data.

Additionally, Athena breaks the fit error into bias, U_B, variance, U_V, and covariance, U_C, proportions as follows[14]:

$$U_B = \frac{(\bar{\hat{y}} - \bar{y})^2}{(1/N)\sum_{i=1}^{N}(\hat{y}_i - y_i)^2}, \qquad U_V = \frac{(\sigma_{\hat{y}} - \sigma_y)^2}{(1/N)\sum_{i=1}^{N}(\hat{y}_i - y_i)^2}$$

$$U_C = \frac{2(1-\rho)\sigma_{\hat{y}}\sigma_y}{(1/N)\sum_{i=1}^{N}(\hat{y}_i - y_i)^2} \tag{14}$$

Where ρ and σ are the correlation coefficient and standard deviation, respectively,

$$\rho = \frac{1}{\sigma_y \sigma_{\hat{y}} N}\sum_{i=1}^{N}(\hat{y}_i - \bar{\hat{y}})(y_i - \bar{y}), \qquad \sigma_x = \sqrt{\frac{1}{N}\sum_{i=1}^{N}(x_i - \bar{x})^2} \tag{15}$$

The bias proportion presents the deviation of the average values of the simulated and measured data acting as a measure of model systematic error. The variance proportion acts as a measure of the model's ability to duplicate the variability in the true system. The covariance proportion is a measure of nonsystematic error, for example, due to unmodeled random sensor/system noise. Note that these three proportions sum to 1, with the ideal fit having U_B and U_V close to zero, with U_C close to 1.

These fit statistics act as a measure of accuracy and/or certainty in the proposed model formulation under investigation and provide clues into the effectiveness, or lack thereof, of adjustments introduced in the model structure.

An additional strength of this algorithm is its ability to analyze multiple segments of information, in this case PID maneuvers, at once. This allows for the extraction of global models from analysis groups of multiple PID maneuvers. Overall, this procedure is a fast, single-pass algorithm that results in good base model structure determination.

Algorithm Application

Athena was employed to extract incremental parameter estimates for aerodynamic body-axis forces and moments given the kinematically consistent dynamic flight data and reconstructed aerodynamic total force and moment coefficients. The ability of Athena to estimate coefficient nonlinearities was exercised by analyzing groupings of PID maneuvers to determine a global aerodynamic model. Sufficient data spanning a range of AOA and sideslip was made available to the algorithm providing a wealth of information. The nonlinear, global model development capabilities of Athena have been exercised with success in prior work.[10]

Recall Athena allows for overall model structures that are linear in the overall parameter buildup but whose individual model terms may be identified to have nonlinear dependencies. Placement of model knot locations is crucial in this process. Knots should be placed within regions where sufficient data are available for the breakpoints in question. In this study, knot locations were predominant for aircraft α and β throughout the force and moment model buildups. As a result, when analyzing a group of PID maneuvers, knot locations for AOA and sideslip were distributed evenly such that they fell within appropriate values for the collective data within that group.

The AOA range collectively spanned by the longitudinal PID maneuvers was 2–12 deg. The AOA and sideslip range collectively spanned by the lateral–directional PID maneuvers was 4–10 and −8–8 deg, respectively. Figure 2 presents the PID flight-test data envelope coverage for the FCL PA-half configuration. In addition, it points out the defined knot locations for AOA and sideslip that were used when estimating the incremental aerodynamic model using Athena. When estimating longitudinal model parameters Athena knots were defined from 2 to 12 deg α every 2 deg. Similarly, when estimating lateral–directional parameters, or longitudinal parameters containing a sideslip dependence, Athena knots were defined from 4 to 10 deg α every 2 deg and −8 to 8 deg β every 2 deg.

Recall the parameter estimation scheme employed in this study is equation error and not an output error technique. Consequently, because of the nature of the estimation technique, each axis for the total force and moment aerodynamic coefficients was examined separately using Athena. That is, the overall models for C_X, C_Y, C_Z, C_l, C_m, and C_n were identified separately. The model structure for each axis was kept as simple as possible to not overparameterize. As already stated, all model terms were identified to contain

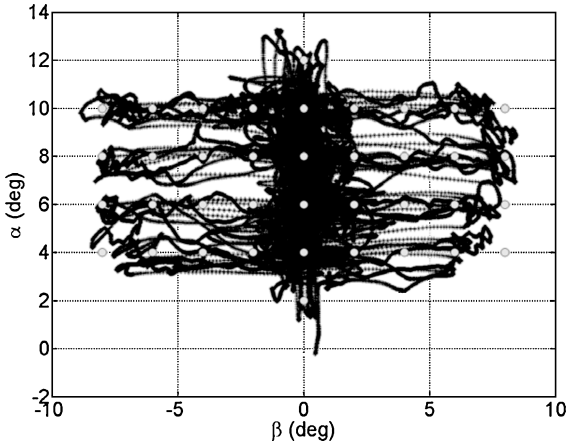

Fig. 2 PID flight-test data envelope coverage for the FCL PA-half, gear-down configuration for all flap splits showing Athena model knot locations.

nonlinear dependencies. However, care was taken to include incremental model terms that would most likely be attributed to an asymmetric LEF split as opposed to estimating an incremental correction term for all possible aerodynamic coefficients present in the baseline model. The correcting increments were formulated based on engineering judgement and qualitative comments recorded by pilots during the flight-test program. The logic behind the increment selection is outlined in the following text.

Consider the special configuration being tested: frozen, off-schedule, and differentially split LEFs. This surely changes the nature of the airflow over the left vs right wing panels and, thus, the main contributor of lift for the aircraft. Inherently, this will have a hand in altering the aircraft lift curve slope as well as pitching moment static stability. In addition, one would expect asymmetric lift and pitching moment characteristics with sideslip of varying sign.

The asymmetric LEF configurations will certainly alter the lateral–directional aerodynamics as well. One might expect the greatest effect of the wing panel asymmetries is to change the basic airframe lateral–directional characteristics. This calls for asymmetric changes in sideforce, directional stability, and dihedral effect with sideslip of varying sign. In addition, a significant amount of asymmetric rolloff tendency while varying AOA would be encountered. Changes to aircraft roll damping and aileron control power were also expected.

Comparison of flight reconstructed total aerodynamic forces and moments with those obtained by overriding the baseline aerodynamic model also reinforced, or provided additional clues, as to where model updates may be required.

A total of 15 nonlinear aerodynamic tables were developed using Athena for the FCL configuration. The final structure for the longitudinal incremental model is shown below and was identified with data spanning the following envelope: 2–12 deg α and −8–8 deg β.

$$\Delta C_Z = \Delta C_Z(\alpha, \delta_{\text{DIFLEF}}) + \Delta C_Z(\alpha, \beta, \delta_{\text{DIFLEF}})$$

$$\Delta C_m = \Delta C_m(\alpha, \delta_{\text{DIFLEF}}) + \Delta C_m(\alpha, \beta, \delta_{\text{DIFLEF}})$$

$$\Delta C_X = \Delta C_X(\alpha, \delta_{\text{DIFLEF}})$$

The final structure for the lateral–directional incremental model is shown below and was identified with data spanning the following envelope: 4–10 deg α and −8–8 deg β.

$$\Delta C_Y = \Delta C_Y(\alpha, \beta, \delta_{\text{DIFLEF}}) + \Delta C_{Y_{\delta_r}}(\alpha, \delta_{\text{DIFLEF}})\delta_r$$

$$\Delta C_n = \Delta C_n(\alpha, \beta, \delta_{\text{DIFLEF}}) + \Delta C_{n_r}(\alpha, \delta_{\text{DIFLEF}})(rb/2V) + \Delta C_{n_{\delta_r}}(\alpha, \delta_{\text{DIFLEF}})\delta_r,$$

$$\Delta C_l = \Delta C_l(\alpha, \beta, \delta_{\text{DIFLEF}}) + \Delta C_{l_p}(\alpha, \delta_{\text{DIFLEF}})(pb/2V) + \Delta C_{l_r}(\alpha, \delta_{\text{DIFLEF}})(rb/2V) + \Delta C_{l_{\delta_{a_l}}}(\alpha, \delta_{\text{DIFLEF}})\delta_{a_l} + \Delta C_{l_{\delta_{a_r}}}(\alpha, \delta_{\text{DIFLEF}})\delta_{a_r}$$

Overall, a total of 15 nonlinear aerodynamic tables were constructed from the identified model. Each table is a consolidation of Athena parameter estimates determined at the specified knot locations. All tables are a function of the differential LEF split and AOA at a minimum. Lateral–directional, and some longitudinal, increments contain a sideslip functionality as well. Knot locations for AOA and sideslip for each model parameter containing them are as defined earlier. In addition, each incremental model term just outlined also contains a dependence on differential LEF deflection (δ_{DIFLEF}). All model correction increments shown provide an output of zero for a differential LEF deflection of zero. Note that linear splines were used in Athena to evaluate the coefficient outputs when navigating between defined knot locations. This spawns from the requirement in the baseline simulation to install all aerodynamic model update terms in the form of structured tables with linear interpolation between the defined table breakpoints. Consequently, the total aerodynamic coefficient comparison matches determined using Athena and those made using the baseline simulation would be identical after final model installation for verification purposes.

Recall there are five flap splits investigated in this study. In addition, as already stated, when estimating longitudinal model parameters, Athena knots were defined from 2 to 12 deg α every 2 deg. Similarly, when estimating lateral–directional parameters, or longitudinal parameters containing a sideslip dependence, Athena knots were defined from 4 to 10 deg α every 2 deg and −8 to 8 deg β every 2 deg.

The body Z-axis force and pitching moment incremental models contain the basic airframe term $[\Delta C_{Z,m}(\alpha,\delta_{\text{DIFLEF}})]$, as well as an increment due to sideslip $[\Delta C_{Z,m}(\alpha,\beta,\delta_{\text{DIFLEF}})]$. The sideslip increment was constrained to zero for $\beta = 0$ deg during identification. Overall, these nonlinear tables were identified using longitudinal 3–2–1–1s and SHSSs. The inclusion of SHSS maneuvers in the identification process allows for the determination of sideslip effects on lift and pitching moment. The final tables for $[\Delta C_{Z,m}(\alpha,\delta_{\text{DIFLEF}})]$ were constructed from 30 parameters each, whereas the final tables for $[\Delta C_{Z,m}(\alpha,\beta,\delta_{\text{DIFLEF}})]$ were constructed from 160 parameters each, as estimated by Athena. Recall the table entries corresponding to $\beta = 0$ deg for the latter tables were fixed to zero and not estimated by Athena.

Comparisons between flight reconstructed aerodynamic body X-axis forces and histories predicted by the baseline aerodynamic model indicated the need for a drag correction increment. Predictions from the baseline simulation were found to be consistently lower in magnitude than those reconstructed from flight-test data. Consequently, a body X-axis force incremental coefficient was included in the estimation process $[\Delta C_X(\alpha,\delta_{\text{DIFLEF}})]$. This correcting increment was identified using longitudinal 3–2–1–1 maneuvers. The final table for $[\Delta C_X(\alpha,\delta_{\text{DIFLEF}})]$ was constructed from 30 parameters estimated by Athena.

The body Y-axis force and yawing moment incremental models contain a basic airframe term $[\Delta C_{Y,n}(\alpha,\beta,\delta_{\text{DIFLEF}})]$, as well as a rudder power correction term $[\Delta C_{Y\delta r,n\delta r}(\alpha,\delta_{\text{DIFLEF}})]$. The rudder power incremental update was small in magnitude and is considered a possible improvement to the baseline model as opposed to aerodynamic influences caused by the degraded LEF configurations. A yaw damping incremental term was also necessary $[\Delta C_{nr}(\alpha,\delta_{\text{DIFLEF}})]$ due to the degraded LEF configurations. Although the vertical tail typically poses the largest contribution to yaw damping, recall there is an aircraft wing–body contribution.[15] The wing–body effects are typically caused by increasing drag experienced by the wing resulting from relative wing panel velocities imparted by yaw rate. The inclusion of these terms offered the most significant impact on the Theil fit statistics for model improvement. Overall, the side force and yawing moment incremental models were identified using directional 3–2–1–1 and SHSS maneuvers. The final tables for $[\Delta C_{Y,n}(\alpha,\beta,\delta_{\text{DIFLEF}})]$ were constructed from 180 parameters each, as estimated by Athena. Final tables for $[\Delta C_{Y\delta r,n\delta r}(\alpha,\delta_{\text{DIFLEF}})]$ and $[\Delta C_{nr}(\alpha,\delta_{\text{DIFLEF}})]$ were constructed from 20 parameters each, as estimated by Athena.

The most significant rolling moment coefficient changes occurred within the basic airframe incremental coefficient $[\Delta C_l(\alpha,\beta,\delta_{\text{DIFLEF}})]$. Adjusting increments for roll damping $[\Delta C_{lp}(\alpha,\delta_{\text{DIFLEF}})]$ and rolling moment due to yaw rate $[\Delta C_{lr}(\alpha,\delta_{\text{DIFLEF}})]$ were also identified. The predominant contribution to roll damping is typically affected by the wing–body configuration.[15] The wing–body contribution to roll damping arises from the change in local wing panel AOA, and thus wing panel lift, caused by body axis roll rate. The wing–body configuration also has an affect on rolling moment due to yaw rate.[15] This typically arises from the change in lift experienced by the wing resulting from relative wing panel velocities imparted by yaw rate. Finally, an incremental correction coefficient was estimated for the rolling moment control power for the left and right ailerons, respectively $[\Delta C_{l\delta ar,l}(\alpha,\delta_{\text{DIFLEF}})]$. The rolling moment incremental model was developed using lateral 3–2–1–1, SHSS, and longitudinal 3–2–1–1

maneuvers. The inclusion of the longitudinal maneuvers assisted in the identification of the basic airframe rolling characteristics with variations in AOA. The longitudinal 3–2–1–1s were flown without the pilot arresting rolloff due to AOA perturbations by design. The final table for $(\Delta C_l(\alpha,\beta,\delta_{\text{DIFLEF}})]$ was constructed from 180 parameters estimated by Athena. Final tables for $[\Delta C_{lp}(\alpha,\delta_{\text{DIFLEF}})]$, $[\Delta C_{lr}(\alpha,\delta_{\text{DIFLEF}})]$, and $[\Delta C_{l\delta ar,l}(\alpha,\delta_{\text{DIFLEF}})]$ were constructed from 20 parameters each, as estimated by Athena.

Implementation of the incremental aerodynamic model update entailed installing the new data tables within the engineering simulation using appropriate CASTLE simulation environment format. In addition, the model structure buildups outlined earlier were added to the overall baseline aerodynamic model total coefficient buildups such that

$$C_{i,\text{total}} = C_{i,\text{baseline}} + \Delta C_{i,\text{Athena}} \tag{16}$$

Where $i = X, Y, Z, l, m$, and n.

Evaluation of Results

Theil Statistics

Figures 3 and 4 present Theil statistic data for the FCL longitudinal and lateral–directional models, respectively. The overall Theil coefficient U, systematic error proportion U_B, variance error proportion U_V, and covariance error proportion U_C are presented for each total aerodynamic coefficient as shown. In both Figs. 3 and 4, the left column presents the Theil statistical information for the baseline aerodynamic model as compared to the total aerodynamic coefficients extracted from flight data. The right column presents the same statistical information for the updated aerodynamic model as compared to total aerodynamic coefficients extracted from flight data. Each graph contains a series of five bars. Each bar, from 1 to 5, corresponds to the statistics for the −5/5 deg, 0/5 deg, 10/5 deg, 20/5 deg, and 34/5 deg LEF split configurations, respectively. Each bar indicates the overall Theil statistic information computed for that particular flap split. Each bar was computed using all maneuver segments employed in the identification of the aerodynamic coefficient model in question for the particular flap split.

Statistics presented in Figs. 3 and 4 indicate the updated model for the FCL configuration has significantly reduced the overall Theil coefficient U (first from top in each set), thus, indicating an increase in fidelity. In addition, it is clear from Figs. 3 and 4 that a significant amount of systematic error U_B (second from top in each set) was removed with the addition of the new model increments. In general, systematic error is most commonly reduced through updates of aerodynamic biases and basic airframe static coefficients ($C_{L\alpha}$, $C_{m\alpha}$, $C_{n\beta}$, $C_{l\beta}$, $C_{Y\beta}$, etc.) as well as control effectiveness coefficients. Reduction in aerodynamic systematic error produces higher fidelity airframe simulation trim characteristics as compared to the actual aircraft. Variability error U_V (third from top in each set) was also reduced throughout. Although the baseline aerodynamic database was indicating somewhat lower levels of this error, as seen in the bar graphs, the increase in model variability fidelity with the new model is noticeable. Variability error may also be reduced through updates of basic airframe static coefficients and control effectiveness, as noted earlier for systematic error, in addition to dynamic and damping coefficients (C_{mq}, C_{lp}, C_{nr}, etc.). In general, reduction of aerodynamic variability error produces higher fidelity airframe simulation response to control inputs, as well as airframe transient response such as short-period and Dutch roll modes. Also of note is the significant increase in the covariance error proportion U_C (fourth from top in each set) toward the ideal condition of 1.0 indicating improvement of the updated model in comparison with the baseline aerodynamic model. Model error proportioned into U_C encompasses such entities as unmodeled random sensor/system noise.

Theil statistic data for the body axis C_X coefficient indicate the majority of improvement lies in the reduction of model systematic error as indicated in Fig. 3a. The PID process estimated a definite increase in aerodynamic drag for all configurations examined given the current propulsion model available for this analysis. The authors

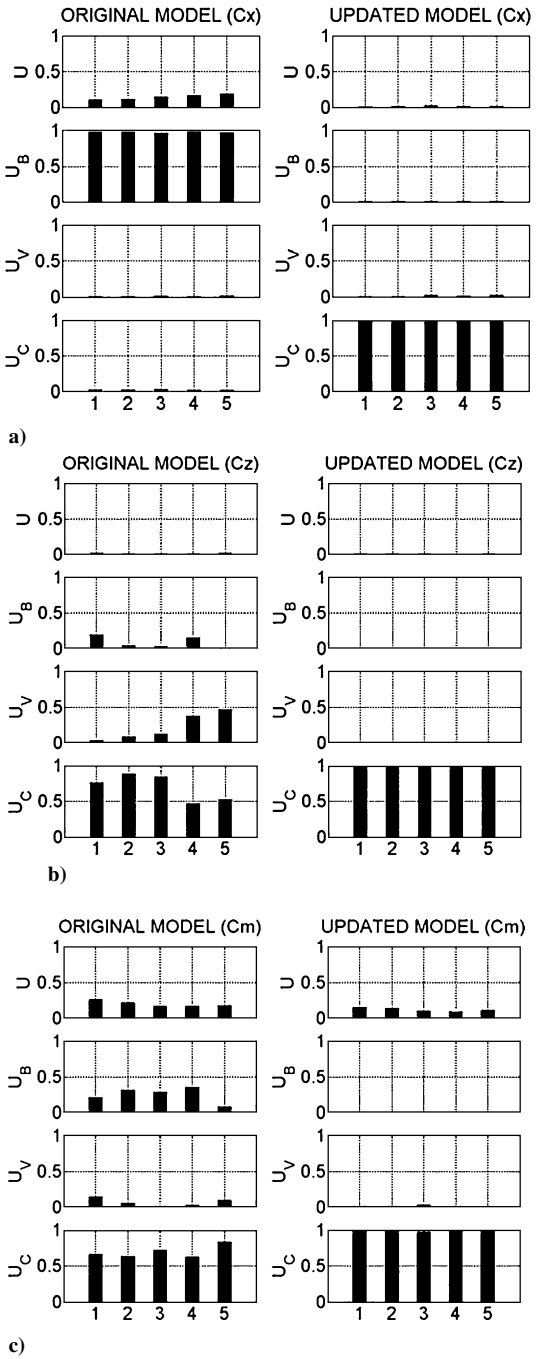

Fig. 3 FCL configuration, longitudinal Theil coefficient results for a) C_X, b) C_Z, and c) C_m.

have high confidence in the baseline drag database within the simulation. Consequently, this required drag increase is most likely due to an overpowered propulsion model.

The baseline aerodynamic database was found to best represent the body axis C_Z aerodynamic coefficient with smaller changes required here overall, as indicated in Fig. 3b. However, a growing variability error when using the baseline aerodynamic model is clearly evident in the Theil data because the left LEF deflection increases in the leading-edge down (positive) sense.

Figure 3c indicates the majority of improvement for body-axis pitching moment C_m was achieved through the removal of systematic error, although a smaller amount of variability error was corrected as well.

Theil statistic data for body-axis side force C_Y is shown in Fig. 4a. The model update removed a significant systematic error that was present at the 20/5 and 34/5 deg LEF split configurations

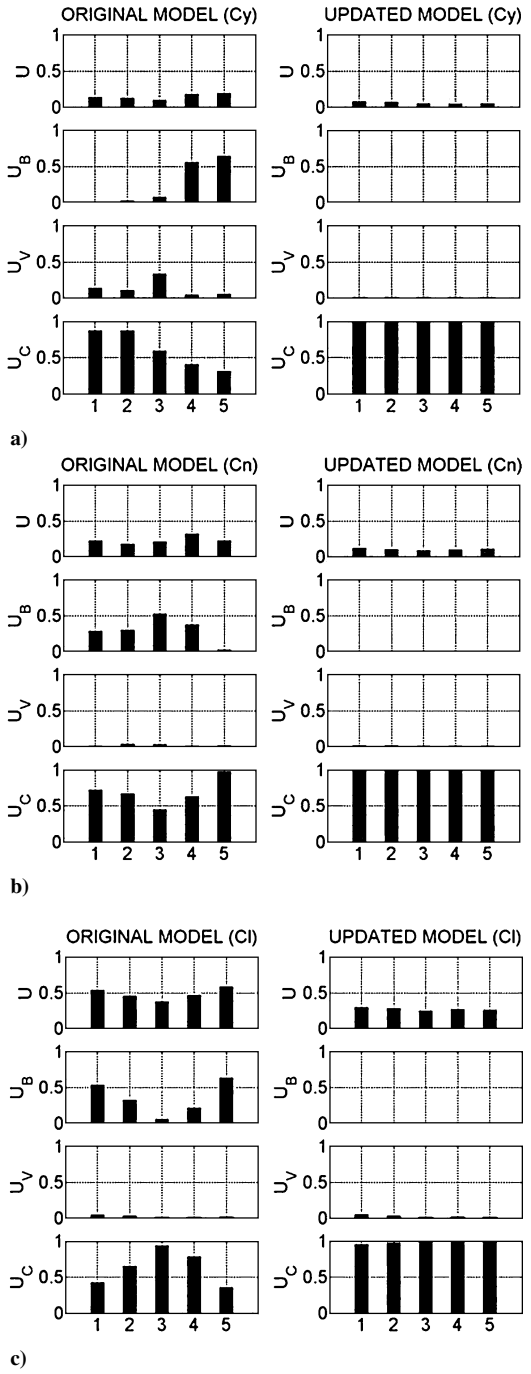

Fig. 4 FCL configuration, lateral–directional Theil coefficient results for a) C_Y, b) C_n, and c) C_l.

when using the baseline aerodynamic model. In addition, significant variability error was reduced at the remaining split LEF configurations.

The majority of improvement in the body-axis yawing moment coefficient model C_n was found to be the removal of significant levels of systematic error. As shown in Fig. 4b, the original model offered a good match for the system variability.

Improvement was made in the fidelity of the rolling moment coefficient model C_l. As shown in Fig. 4c, a significant amount of systematic error was removed with the new model.

Overall, Theil statistic data for the updated longitudinal and lateral–directional model terms, shown in Figs. 3 and 4, indicate the majority of model error present is nonsystematic in nature and falls within the covariance proportion U_C. Again, this is apparent with U_C for the updated model being consistently and, significantly, closer to the ideal condition of 1.0, indicating improvement of the updated model in comparison with the baseline aerodynamic model. Again, U_C encompasses such entities as random sensor/system noise, and the like. In such an analysis it is preferential to attribute the remaining model error to this category. Note that airframe buffet was experienced during the test flights and was found to increase in intensity with AOA. The updated aerodynamic model does not emulate the unsteady aerodynamic buffet effects. Consequently, with the majority of model error for the new model being categorized in the covariance proportion U_C, it is clear the presence of unmodeled airframe buffet is a major contributor to the resulting U_C error proportion.

Aerodynamic Model Sweeps

Figure 5 presents sample aerodynamic model sweeps for the nondimensional rolling moment and pitching moment coefficients for the 34/5 deg split LEF case. The original and updated simulations were configured with fixed control surface positions, as indicated in Fig. 5, in the PA-half, gear-down configuration. The AOA was sequentially set at 4, 6, 8, and 10 deg with sideslip varied from −10 to 10 deg.

Figure 5a presents sweep comparison results for the total aerodynamic rolling moment coefficient. The nonlinear, asymmetric corrections within the updated model are clearly evident. In addition, the new model predicts a change in rolloff direction with zero sideslip taking place between 4- and 6-deg AOA. Figure 5a also indicates a change in roll trim is required at zero sideslip over what was necessary in the original model.

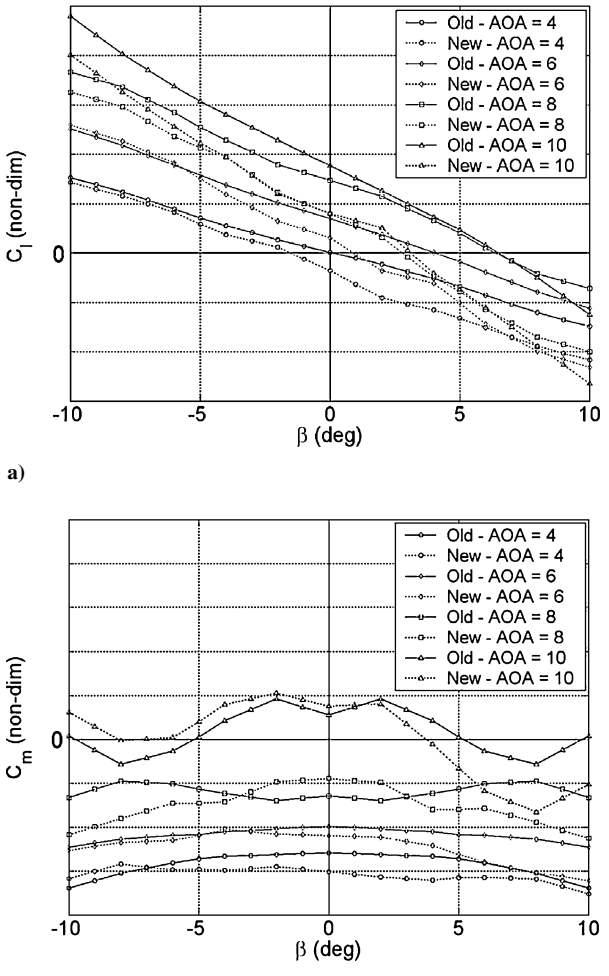

Fig. 5 LEF 34/5 deg FCL half-flaps configuration with gear down at Mach 0.25, total aerodynamic coefficient model sweep for a) C_l and b) C_m.

Figure 5b presents a similar comparison for the total aerodynamic pitching moment coefficient. The longitudinal aerodynamics in the original model approximated symmetrical output with sideslip while in the investigated asymmetric LEF modes. The updated model clearly presents asymmetric influences as would be expected in this off-nominal configuration. In the example shown, a higher nose-down pitching moment (negative) is experienced when side slipping into the LEF with 5-deg deflection (positive sideslip).

Coefficient Comparisons via Model Override

Figures 6 and 7 present all-axis total aerodynamic force and moment coefficient matches for a SHSS maneuver flown at 4- and 10-deg AOA, respectively for the 34/5 deg LEF split configuration. A comparison is made between total aerodynamic forces and moments extracted from flight and those predicted by the original and updated aerodynamic models within the simulation. Predicted aerodynamic histories were acquired by overriding aircraft states, responses, and control surface positions in the CASTLE simulation aerodynamic model with flight data stored in IDEAS. Resulting aerodynamic force and moment coefficients were recorded in the IDEAS database.

Both examples indicate an appreciable increase in fidelity over the original model. Also of interest is the increase in the apparent noise frequency and amplitude present in the lift, pitching moment, and rolling moment coefficients for the 10-deg AOA, case of Fig. 7 over the 4-deg AOA case of Fig. 6. This is no doubt an indicator of the increase in buffet detected by pilots during flight test. In general, buffet encountered was found to increase in severity with AOA. The simulation was not updated to model buffet characteristics. As already mentioned, a significant amount of the nonsystematic, covariance proportion U_C, Theil statistic error encountered by the updated model is no doubt caused by these unmodeled buffet effects.

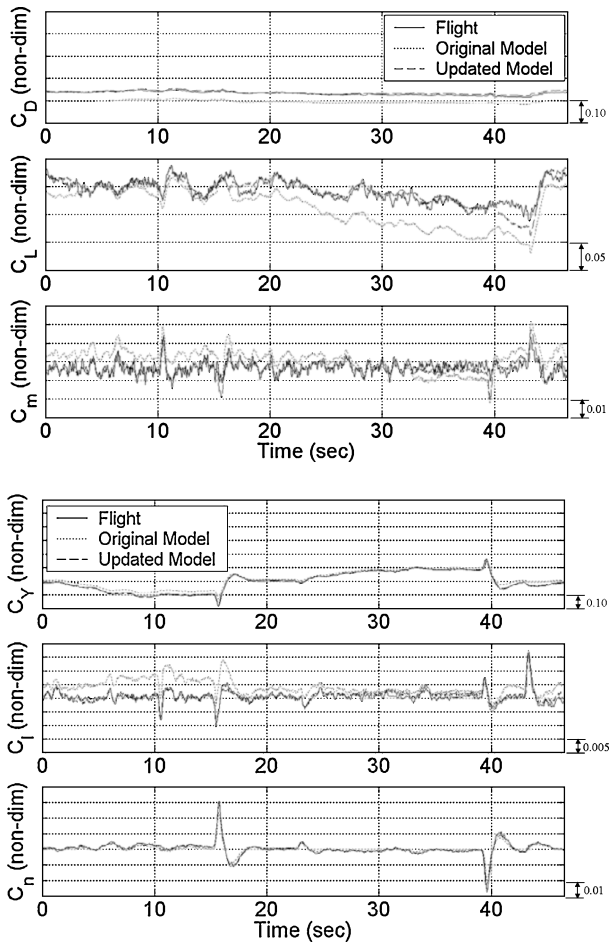

Fig. 6 Aerodynamic coefficient comparison for a steady heading sideslip maneuver at 4-deg AOA with differential LEF split of 34/5 deg for FCL configuration.

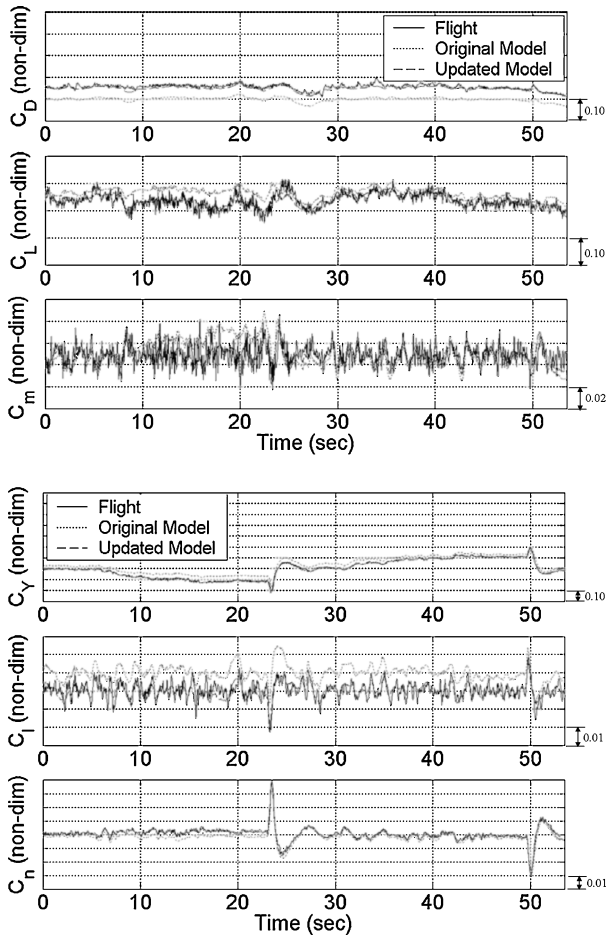

Fig. 7 Aerodynamic coefficient comparison for a steady heading sideslip maneuver at 10-deg AOA with differential LEF split of 34/5 deg for FCL configuration.

Simulation Propagation Comparisons

A final test of model fidelity entails the use of simulation propagation with outputs compared to flight data. On completion of PID analysis, both the original and updated aerodynamic models were available in the CASTLE airframe simulation. Flight-test measurements for pilot longitudinal/lateral stick, pedal, and throttle inputs were used to override pilot control inputs in the simulation. The atmospheric model within the CASTLE simulation was initialized to flight-test conditions. Constant atmospheric winds were set to estimates obtained during NAVIDNT kinematic consistency studies per maneuver. Aircraft weight and balance information, including c.g., etc., were initialized to data made available from the flight-test program per maneuver based on actual loadings. Before propagation, the simulation was trimmed to match any nonsteady initial conditions $\dot{u}$, $\dot{v}$, $\dot{w}$, $\dot{p}$, $\dot{q}$, and $\dot{r}$ in the test data. In addition, the simulation was initialized with the appropriate LEF split, airspeed, altitude, body-axis angular rates, and Euler attitudes as determined from the flight data.

Because of the configurations examined in this study, the lateral–directional axes indicate the greatest magnitude of improvement. Figures 8 and 9 present original and updated model propagation results compared to flight data for a SHSS and lateral 3–2–1–1, respectively, for a 34/5 deg LEF split. Note that all histories presented in Figs. 8 and 9 have been normalized by the absolute maximum magnitude of the flight-test signal for each plot. Figures 8 and 9 offer a general overview of the increase in model fidelity of the updated model vs the original model.

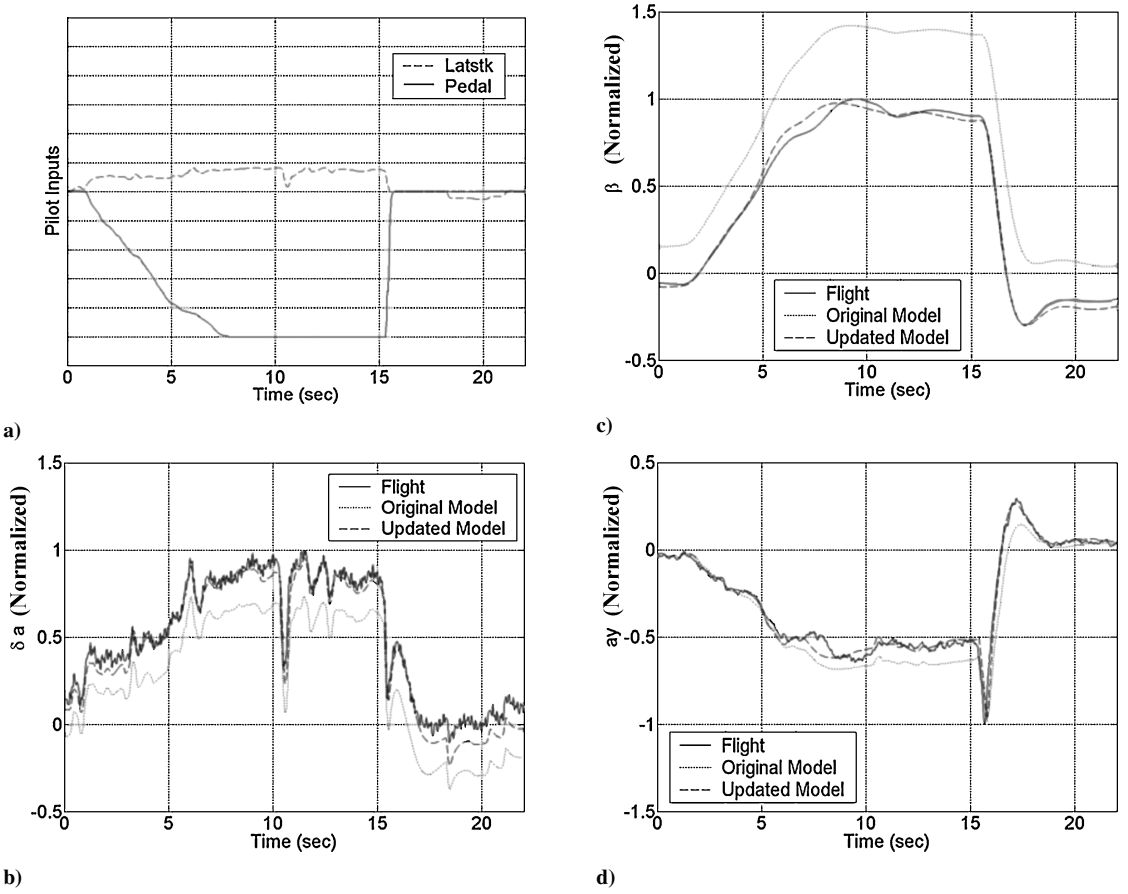

Fig. 8 Propagation comparison between original and updated model for a SHSS maneuver with LEF 34/5 deg split; all histories normalized with respect to absolute maximum magnitude of flight data.

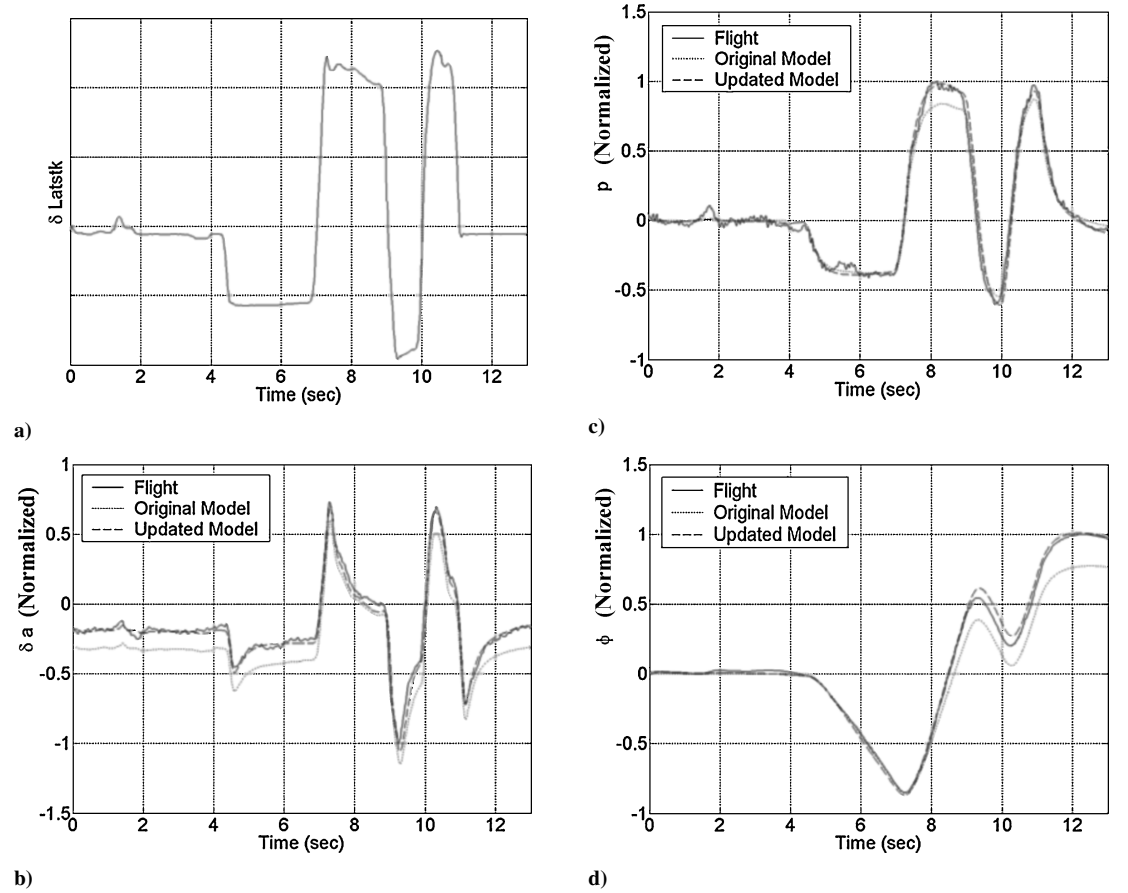

Fig. 9 Propagation comparison between original and updated model for a lateral 3–2–1–1 maneuver with LEF 34/5 deg split; all histories normalized with respect to the absolute maximum magnitude of flight data.

As in any standard SHSS maneuver, Fig. 8a shows the gradually applied pedal input to build sideslip while lateral stick cross control is applied maintaining heading. Figure 8b is an excellent indication of the systematic error removed from the rolling moment aerodynamic model. The updated overall aileron deflection indicates a clear improvement for initial trim position as well as throughout the span of the maneuver. Figure 8c presents the match for sideslip angle with definite improvement for the updated model over the original model. Systematic error, based on β during the trim phase, is clearly reduced. In addition, a reduction in variability error is noticeable in the updated model over the original model. This is indicated by the overshoot in β encountered by the original model and, most important, the transient response differences resulting from abrupt control release. The original model indicates higher transient response damping than flight. In addition, the original model trimmed to a different sideslip angle, as compared to flight data, to obtain the initial flight lateral acceleration as shown in Fig. 8d. Both the original and updated model computed a_y matches well with flight test as the gradual pedal input begins. However, the original model overshoots the flight a_y at peak β as well as results in a higher damped transient response than flight.

Figure 9a shows a sample lateral stick input for a 3–2–1–1 maneuver. A reduction in systematic error for the rolling moment aerodynamic model is again indicated by the bias that has been removed from the overall aileron deflection as shown in Fig. 9b. Less aileron deflection is required for trim by the updated model, and flight, as compared to the original aerodynamic model. Figures 9c and 9d compare original and updated model responses for body axis roll rate p and roll attitude ϕ to flight data. These history comparisons indicate a clear reduction in variability error of the updated model over the original model. Changes in parameters such as airframe roll damping and aileron lateral control power have contributed to a higher fidelity roll response for the updated model.

Conclusions

The MFS facility of NAVAIR at the Patuxent River Naval Air Station has supported flight-test preparation and aerodynamic modeling efforts for the split LEF degraded modes study for the F/A-18E aircraft. Support consisted of PID maneuver design, flight-test pilot preparation, flight-test support, and subsequent aerodynamic model development.

This work resulted in the development of nonlinear model updates for the FCL configuration with LEF splits of $-5/5$ deg, $0/5$ deg, $10/5$ deg, $20/5$ deg, and $34/5$ deg. The updated model was flown at MFS by pilots to obtain, or refresh, familiarity with the aircraft flight characteristics for the FCL LEF degraded modes before phase 2 of this testing. Phase 2 of this continued flight-test program took place during shipboard operations at sea.

References

[1]Linse, D. J., "Aircraft System Identification Using Integrated Software Tools," *Proceedings of the Research and Technology–Systems Concepts and Integration Symposium*, Madrid, Spain, May 1998; also Paper No. 11.

[2]Linse, D. J., "Improving Simulator Accuracy with Integrated Analysis of Flight Data," Interservice/Industry Training, Simulation, and Education Conf., I/ITSEC Paper EC-046, Nov. 2000.

[3]Paris, A. C., and Alaverdi, O., "Post-Flight Inertial and Air-Data Sensor Calibration," AIAA Atmospheric Flight Mechanics Conf., Boston, MA, AIAA Paper 98-4450, Aug. 1998.

[4]Dennis, J. E., Jr., Gay, D. M., and Welsch, R. E., "An Adaptive Nonlinear Least-Squares Algorithm," *ACM Transactions on Mathematical Software*, Vol. 7, No. 3, 1981, pp. 348–368.

[5]York, B. W., Magyar, T. J., and Nichols, J. H., "CASTLE: The Next Generation of Navy Flight Simulation," AIAA Paper 2001-4243, Aug. 2001.

[6]Koehler, R., and Wilhelm, K., "Auslegung von Eingangssignalen für die Kennwertermittlung," DFVLR-IB 154-77/40, DFVLR Inst. für Flugmechanik, Brunswick, Germany, Dec. 1977.

[7]Hamel, P. G., and Jategaonkar, R. V., "The Evolution of Flight Vehicle System Identification," CP-566, AGARD, Paper 19, Nov. 1995.

[8]Maine, R. E., and Iliff, K. W., "Application of Parameter Estimation to Aircraft Stability and Control—The Output-Error Approach," NASA RP-1168, June 1986.

[9]Bonner, M. S., and Gingras, D. R., "Evaluation of the Navy's F/A-18A/D Powered Approach Aerodynamics Model," AIAA Paper 97-3667, Aug. 1997.

[10]Paris, A. C., and Alaverdi, O., "Nonlinear Aerodynamic Model Extraction from Flight Test Data for the S-3B Viking," AIAA Paper 2001-4015, Aug. 2001.

[11]Anderson, D. M., DeMand, R. P., Klein, D. J., Sherman, S., Moomaw, R. F., Bloemker, E. B., Diecker, R. D., Pulley, C. M., and Shirk, F. J., "F/A-18E/F Flying Qualities Report," The Boeing Co., Rept. Boeing-STL 99A0070, St. Louis, MO, Jan. 2001.

[12]Anderson, L. C., "Robust Parameter Identification for Nonlinear Systems Using a Principal Components Regression Algorithm," AIAA Paper 85-1766, Aug. 1985.

[13]Linse, D. J., "System Identification Software Design Document and User's Manual for the Integrated Data Evaluation and Analysis System (IDEAS)," Science Applications International Corp., SAIC Rept. 01-1393-2990-A005/A006, Lexington Park, MD, Nov. 1997.

[14]Pindyck, R. S., and Rubinfeld, D. L., *Econometric Models and Economic Forecasts*, 3rd ed., McGraw–Hill, New York, 1991, pp. 336–342.

[15]Roskam, J., "Airplane Flight Dynamics and Automatic Flight Controls—Part I," Roskam Aviation and Engineering Corp., Ottawa, KS, 1982, pp. 195–197, 203–205.